09/29/93

The Future of Geomagnetic Storm Predictions: Implications from Recent Solar and Interplanetary Observations

Bruce T. Tsurutani
Jet Propulsion Laboratory

and

Walter D. Gonzalez*
Instituto National Pesquisas de Espaciais (INPE)

* Visiting at Space Environment Laboratory, National Oceanic and Atmospheric Administration, Boulder, Colorado 80303

ABSTRACT

Within the last 6-7 years, there has been a substantial growth in our knowledge of the solar and interplanetary causes of geomagnetic storms at Earth. This review article will not attempt to cover all of the work done during this period. This can be found elsewhere. Our emphasis here will instead be on recent cutting-edge efforts that expose important, presently unanswered questions that must be addressed and solved before true predictability of storms can be possible. Hopefully, this article will encourage some of readers to join in on this effort and perhaps make major contributions to the field.

INTRODUCTION

We now know that intense ($D_{ST} \leq -100$ nT) geomagnetic storms are caused by large southward interplanetary Bz events ($B_z \leq -10$ nT) that have durations equal to or greater than 3 hours (Gonzalez and Tsurutani, 1987). These events are typically associated with high speed solar wind streams (Burlaga et al., 1987; Tsurutani et al., 1988; Gosling et al., 1991) that are the interplanetary extension of coronal mass ejections (CMEs), impulsive events occurring at the Sun.

A few years back, it was "common knowledge" that magnetic reconnection occurred in solar active regions creating solar flares and the concomittal expulsion of coronal mass outward from the Sun. However, careful coronagraph data studies (Harrison, 1986; Harrison, 1991) have shown that CMEs are accelerated as they propagate outward, and the initial release time of the CME thus actually precedes the time of onset of the related solar flare and/or prominence eruption. Thus, the release of CMEs (or their related mechanism), must be the cause of solar flares rather than vice-versa. These new observations have caused a flood of new ideas on the release mechanism for CMEs. The mechanism is still not well understood, but one promising ideas is the presence of strong sheer forces together with magnetic buoyancy may allow the release of previously bound coronal mass (Low and Smith, 1993). We will come back to this idea somewhat later.

Below, we willattempt to summarize some of the most recently published work and ideas to give the reader a view of our present understanding regarding the solar, interplanetary and magnetospheric physics associated with magnetic S(01111S.

Coronal Mass Ejections

Hundhausen (1993), in a recent outstanding paper, has examined over 1300" coronal mass ejections from the Solar Maximum Mission coronagraph/polarimeter images of the solar corona. The data spans 1980 and 1984 through 1989. Hundhausen (1993) finds that the CMEs' latitude distribution is clumped about the heliomagnetic equator, rather than around the heliographic equator. The CME latitude distribution is therefore different from that of sunspots, active regions and/or Hα flares. He finds that the average angular width of a CME is 4-/" with a median value of 44".

Perhaps the most encouraging result that Hundhausen (1993) has discovered 1"01 stor 111 predictability is that there are often visible signals preceding the release of CMEs. Figure 1 is a synoptic map of the east limb (top) and west limb (bottom) of the corona at a distance of $2R_S$ from the center of the Sun. Time increases 10 the left. The bright regions correspond 10 coronal helmet streamers, closed magnetic field regions, closely corresponding to the magnetic equator. Also indicated in the Figure are location (dots) where the CME events have taken place. The CME angular widths are indicated by vertical bars. What is quite striking in the Figure is that one can note that coronal mass ejections typically come from the helmet streamer belt and there is often a preceding brightening and broadening of the local steamer belt prior IO CME release. After the release, the local streamer belt at the CME release site dims substantially.

Such a visible precursor, indicative of an impending release of coronal mass, gives hope that we can eventually predict geomagnetic storms days 01 even weeks before Inc. coronal mass is actually ejected. This advanced warning is in addition to the 1-3 day propagation time for the interplanetary disturbance to reach the Earth.

There are, however, presently limitations 100111 knowledge about when CMEs will be released. Only about half of the CMEs used in the SMM study showed this prior brightening and broadening (Hundhausen, 1993). '1'1](".11' is also no obvious coronal feature that presently can be used to predict the velocity of the CME well away from the Sun (whether it will be fast enough to produce a shock wave or not), nor is there any obvious coronal feature or features that can be used to predict exactly when release will occur (Hundhausen, personal comm., 1993). These are some of the obvious challenges for the solar physicists for the next few years.

Perhaps one important clue that might give physical insight into CME releases has been recently provided by Gonzalez and Tsurutani (1993). Figure 2 shows the relationship between coronal holes, active regions and the heliospheric current sheets (CHARCS). Here, Gonzalez and Tsurutani have examined this relationship for 10 intense magnetic storms that were previously discussed in the literature (Tsurutani et al., 1988; Gonzalez et al., 1989; Tang et al., 1989). The location of the coronal holes (cross-hatched regions) were obtained from the NOAA Boulder Solar Geophysical Data (P. McIntosh, private communication, 1993), the current sheet location (dashed lines) are from Hoeksema and Sherrer (1986) and the active region locations (X's) are from Tang et al. (1989). From the Figure, the reader can note that the active regions (AR) is always to the left (eastward in the Carrington rotation plots) of the current sheet. During the period when these events occurred (1978-1979), close to sunspot maximum (1979), the current sheet had very high (almost vertical) inclinations. Another important feature is that low latitude coronal holes are also present very close to the AR and to the current sheet. At the present time it is not clear what this three-way interrelationship indicates. However, it exists for practically all of the 10 storms studied by Gonzalez et al., (1989) and certainly seems to not be coincidental. One speculation is that the streams associated with the coronal holes may, through nonradial flow, pressurize the fields near the current sheet (the helmet streamer fields) and lead to their destabilization. It should be noted that although the exact location of the CME is not known, it is known to be in the same general vicinity as the AR. Thus, the correlation that Gonzalez and Tsurutani have found also goes fro CMEs as well.

Interplanetary CMEs

A recent schematic of what an interplanetary CME looks like is shown in Figure 3, taken from Choe et al. (199?). The fastest CMEs with associated forward shocks are the events that are most likely to cause intense geomagnetic activity, so this case is illustrated here. Further discussion of CMEs in this paper will concern only the fast events. There are two regions in the vicinity of a CME where there are intense Ills{',tlctic fl('ids, in the sheath regions behind (sunward of) the shock, and in the driver gas (CME) proper. The first region has intense magnetic fields due to the shock compression of the slow, up stream solar wind. The amount of compression depends 011 the shock Mach number (which in turn depends on the relative velocities Of the two streams and the local magnetosonic wave phase speed). The field within the driver gas is outwardly convected plasma from the solar source region. The driver gas is a low beta region ($\beta \leq 0.1$, Choe et al., 1992). Various means of identifying the driver gas have been applied: sensing bidirectional electron and proton streams (Gosling et ill., 1987) detecting high but low variance magnetic fields (Pudovkin and Chertkov et ill., 1976; Zwickl et al., 1977; Tsurutani et

a ., 988), and low plasma temperatures (Zwick et al., 977). should be mentioned ha a universal set of identification criteria have not been found (Zwickl et al., 977; Choe et al., 992), even though serious attempts have been made Identifying drivers is stil a difficult and uncertain task.

Because of this difficulty, an important region of the driver gas has been missed until recently. Choe et al. have found that in about 30% of the cases, there is an outer shel of helium en iched plasma around the high magne ic field region (shown by the cross-latched region in the Figure). he helium to proton density ratios are greater than 10%, with values up to 20%. Somewhat embarrassingly, this feature was the original criterion when driver gases were first identified (Hirschberg et al., 1976). had been overlooked by investigations partially because the He enhancements are spotty (thus the development of the aisin-pudding model), and no one had attemj ted to look for another shel . Whether there is always addi iona driver gas material outside the high field egio is unclear a this ime. At present, the Helium enrichment is only consistent feature ha has been found. A magnetic discontinuity is noted at the outer boundary of the shell, but this discontinuity is not particularly unique and does not appear to be always usable to identify the shell boundary. Shells may therefore be present more often than 30%, but we cannot identify these at present. Furthermore, there may be CME material even beyond the Helium shell. At this time we cannot tell.

The reason that Choe et al. have stated that a "shell" is present is that as the spacecraft penetrated throughout the high-speed stream, the Helium enhancement was identified twice on oth sides of the high field, low beta region. When He is present, it is present in both regions. Detecting both crossings also allowed Choe et al. to determine the shape of the driver gas. They applied the minimum variance technique (Sonnerup and Cahil , 1976) to the high resolution magnetic field data at the (tangential) discontinuities, and obtained the normals to the surfaces. What they obtained is a flattened frontside with a more elongated ailing portion, shown in the schematic.

low does this driver gas correspond to CMEs observed closer to the Sun? We use the Illing and lundhausen (1986) figure of CME as an illustration. This is shown in Figure 4. There are three principa regions almost always present: an outer bright loop or loops, a dark region sunward of the bright loop, and a twisted filamentary structure closest to he Sun What corresponds to what? Our suggestion is that because the CME dark region is devoid of material, it is most probably the igh field low-β region noted in interplanetary space. The low temperature and bidirectional streaming is also consistent with his icture. The bright outer oops of the CME may correspond to the Helium enriched region. A AU the plasma β is ypically ~ .0 in this

I le rich region, so this cor respondence fits quite nicely. If one adopts this scenar io, then there should always be plasma outside of the high field region (there are always br ight loops), and researchers should therefore look carefully to confirm or deny this possibility. Finally, wh at (lo the filament con esponds to in inter planetary space? In this picture the filaments have yet to be identified. If this scenar io is cor rect, these filaments should be located sunwar d of the high field, low β regions.

Prediction of IMF B_z Directionality

If we are able to predict the occur re nce of a high field region propagating towards the Earth's magnetosphere, this is only part of the predictability problem. We also need to predict the direction of the interplanetary magnetic field. It must be substantially southward for magnetic reconnection and intense solar wind en ner gy transfer to the magnetosphere to occur. 1 loeksema and Zhao (1 992) and Zhao et al. (1993) have **USC.** d a potential field m odel of the cor ona to estimate the direction o f the coronal field at 0.03 R_S above the solar active region (or prominence) site. They find that they pr ~.diet the correct orientation of the interplanetary magnetic field driver gas (based on the assumption that the ().()3 R_S fields are simply convected outward) "/ out of 8 times for active regions (ARs), but O out of 1 times for prominences. Although the correspondence is high for active regions, the statistics are still poor. A similar effor t will be carried out in the near future using a greater number of events.

Wc also still need to be able to predict the magnitude of B_S and perhaps even more difficult, the scale. of the str ucture (the length of time that such a field orientation will be maintained as the solar wind **flows** past the magnetosphere). The above also only addresses fields within the driver gas. The sheath fields which are responsible for 50% of major ($D_{ST} \leq$ - 100 nT) storm onsets cannot be predicted by this means.

The seasonal variations for intense magnetic storms that occurred between 1975 and 1986 i s given in Figure 5. This is taken from Gonzalez and Tsurutani (199?). The peak occurrence of storms are found near Ma rch-April and October- November. These two per iods are close to the equinoxes where the Earth 's dipole lilt in the y-direction are maxi ma , and also when the Earth has maximum and minimum h eliocentr ic latitudes. Explanatio ns of the storm seasonal variations have thus fallen into two categor ies, equinoctial and axial hypotheses, r espectively.

Equinoctial Hypothesis

Figure 6 gives some mechanisms for southward sheath fields. There are three in particular (a, d and f) that could be combined to get a seasonal dependence of sheath fields. First, if for some reason, there are southward fields upstream of the shock, shock compression will allow an intensification of this component. Field line draping around an object such as a CME will **lead** to squeezing of the plasma along the lines of force in the antisolar direction, leaving a low β high field region remaining near the nose of the object. 'Thus, if the sheath fields are southward, this Zwan-Wolf (1976) effect will lead to further intensification. During the equinoxes when the Earth's dipole tilt is maximum in the y axis direction, ecliptic B_y fields will attain significant B_z components when transformed to GSM coordinates (Russell and McPherron 1973; Crooker et al., 1992). This plus the other two mechanisms (shock compression plus draping) could lead to significant southward magnetic fields in the sheath region behind the CME shocks.

However, the sign of B_z depends upon the sign of the GSE B_y field. One sign of B_y will lead to greater southward fields in GSM coordinates and the other sign of B_y will decrease 11s. Thus, it is not clear what the overall effect might be for this mechanism.

Gonzalez et al. (1993) have tested the effect of this mechanism for major ($D_{ST} \leq -100$ nT) and great ($D_{ST} \leq -250$ nT) magnetic storms where sheath fields have been clearly identified (Tsurutani et al., 1988; 1992). Examples of two events are shown in Figure 7. For the top event, that of September 18, 1979, there is very little difference between the B_z component in GSM and GSE. This is because the GSE B_y component is very small and the coordinate transformation therefore has only a minor effect 011117,. The GSM B_z is due. to the presence of significant B_z in GSE coordinates.

A second example of a magnetic storm that occurred near a (spring) equinox is shown in the bottom panel. In this case, the coordinate transformation caused the field to be more northward, actually diminishing the storm's intensity.

Gonzalez et al. (1 993) have summarized their study in Table 1. Major storms are listed in part A (top) and great storms in part B (bottom). Both the peak and the (main phase) storm time-integrated B_z fields were considered. These B_z values are shown in both GSE and G S M coordinates. A positive percentage increase indicates that B_z becomes more negative as the fields are transformed from GSE to GSM coordinates.

Several points can be noted in the Table. First consider the peak B_Z values. The effect of the coordinate transformation is mixed. (4 of 9) events increase and the other half (5 Of 9) decrease. Also the percent effect is quite small, considerably less than the maximum effect that Crooker et **ill. (1** 993) indicate is possible. ([he maximum effect occurs when the field is entirely in the GSE B_Y direction and when the local time allows the magnetic dipole. tilt to be in the same sense as the Earth's rotation axis tilt). There are only two events where there is a ≥ ?0% effect on the peak B_Z. This is on March 10, 1979 (-i ? 1.0%) and on April 13, 198 I (- 24.4°).

Gonzalez et al. have also considered the time integrated B_Z value in the sheath region. This was calculated on the presumption that these might be a "priming" effect on the magnetosphere. 1 lowever, any such priming effect must be quite short lived, and this integration is thus an upper limit to the effect. Gonzalez et al. (] 989) have shown that the peak southward B_Z values occurs within 1-2 hours of the peak D_{ST} and they and Feldstein (1992) estimate that the ring Current decay rate near the peak D_{ST} is ~ 1 hour 01 less. Thus integration times Of only one or two hours are realistic. In the Table, 6 of 9 events are helped by the coordinate transformation. Again, there are only two events with ≥ ?0% effects. They are the September 29, 1978 event (43.?%), and the February 21, 1979 event (- 21.5%).

We conclude that the equinoctial hypothesis is valid and can influence B_Z, particularly for those causing smaller fields related to substorms. 1 lowever, there is no compelling evidence that this mechanism can explain the wry large seasonal modulation of D_{ST} shown in 1 figure 5. For about half of the major and great storms, it can influence the B_Z field at a 10-?0% level at best, and it both increases and decreases B_Z and the size Of the storm. Therefore, other mechanisms must be sought for this modulation.

Axial 1 lypothesis

Because of the lack of the effectiveness Of the equinoctial mechanism to create the intense southward fields for major magnetic storms, we reexamine the possibility that axial mechanisms are the dominant cause of this effect. For this mechanism, **WC** focus **011** the driver gas fields rather than the sheath fields.

Figure 8 shows the location of five solar source regions where the driver gas fields from the CMEs produced major 01' great magnetic storms at Earth. The latitude Of the Earth has been subtracted out. From **the** Figure we note that all **of** the solar sources are close **to** the latitude Of the Earth and longitudinally are close to the central meridian (CM) plane. The previously

reported average angular width of CMEs close to the Sun of 44° (Lundhausen, 1993) is consistent with this distribution and the assumption that the CME propagates radially outward from the Sun. The angular width of the associated shock is ~ 90°, considerably broader.

The orientation of the field within the driver gas is generally unknown. However, for the cases where the fields cause intense magnetic storms, the field configuration is typically of a magnetic cloud configuration (Klein and Burlaga, 1982), where there are large north-south field components (by definition). Marubashi (1986) has indicated one possible three-dimensional configuration, that of a large magnetic flux-rope. Noting that the B_Z fields are not always the largest at the edges of the magnetic cloud, we have slightly altered Marubashi's figure in Figure 9. This is a multiple flux rope where the inner rope is more intense than the outer one.

With this configuration in mind, Figure 10 illustrates how magnetic clouds could cause geomagnetic effects that are seasonally dependent. One-quarter of the edge of a flux rope is shown. If the spacecraft/Earth cuts through the center of the flux rope (along the x-axis), the B_Z values are maximum, $B_Z = |B|$. If the spacecraft/Earth cuts through point (1), the field is entirely in the B_X direction and there will be only small geomagnetic effects. Therefore, from this schematic, for intense geomagnetic storms, the solar event should take place when the Earth is close to its subsolar point. The finite size of the CME dictates that for substantial B_Z values the CMEs should intersect the Earth's magnetosphere close to its latitudinal center. The motion of the Earth to higher and lower latitudes near the solstices help this to happen.

Viscous Interaction

Thus far we have only been discussing solar wind energy transfer to the Earth's magnetosphere when magnetic reconnection (IMF B_S) is taking place. However, there is another possible mechanism for energy injection, that of a viscous-like interaction. The exact mechanism (Axford and Hines, 1964) is not specified, but a number of more recently suggested possibilities exist.

The Kelvin Helmholz instability has maximum growth rate when the interplanetary fields are oriented orthogonally to the Earth's field. For northward directed interplanetary fields, these will be orthogonal to the geomagnetic tail field. This configuration also minimizes reconnection at the magnetopause (OSL). We feel that these types of events are excellent ones to examine to get an estimation of the level of efficiency for viscous interaction.

For pressure balance at the magnetopause, we use the Spreiter et al. (966) relationship:

$$k\rho\ V_{SW}^2 \cos^2 0: (fB)^2/8\pi \qquad (1)$$

in the above expression, k is the specular reflection index, p the solar wind density, V_{SW} the solar wind velocity, and θ the angle of the solar wind to the magnetopause normal. on the right-hand side. of the equation, B is the magnetopause field strength and f the compressional amplification factor. We use. the empirically determined value of 1.69 for f^2/k (Holzer and Slavin, 1978). We also need to estimate the field at the **dawn and dusk** meridian magnetopause distance relative to the subsolar distance. Sibeck et al. (1991) from an empirical study, has found this expansion factor to be -- 1.1. We will use this number in our calculations.

We also need an expression for the energy dissipation within the magnetosphere. The Akasofu (198 1) expression is

$$U_T = U_O + U_A + U_J \qquad (2)$$

where U_T is the total energy input into the magnetosphere which is composed of the ring current injection energy (U_O), aurora] particle precipitation (U_A) and joule heating (U_J). Akasofu empirically found that U_A **-- 1** x 10^{15} AE (nT) ergs s^{-1} and U_J was twice this value.

Table 2 gives the solar wind data for 1] B_N events identified by Gonzalez and Tsurutani (1986). All of these events were associated with high speed streams during and near solar maximum. The columns, from left-to-right, are the date **of the** event, the **peak** B_N **value, the** duration of the event in hours, the peak magnetic field magnitude of the event, the. Magnetosonic Mach number (if a shock was present), the lag time of the peal B_N relative to the solar wind event onset, the AE value during the event, the D_{ST} value (R indicates recovery phase), the solar wind velocity, proton" density, helium density and the 1 MF B_y values.

in Table 3, the values in "1'able 2 are used to compute some physical parameters. Column 2 is the magnetic field magnitude at the magnetopause nose, calculated from the pressure balance expression given in equation (1). Column 3 is the calculated area of the magnetosphere, column 4 the solar wind energy flux density, and column (5) the energy impinging on the magnetosphere in ergs s]. In comparison, column 1 of Table 4 gives the magnetospheric energy deposition taken from expression (2). The second column of '1'able, 4 is the efficiency of solar wind energy transfer. Typical numbers are 1-3.5 x 10^{-3}. In comparison, for magnetic storms, where

reconnection is the predominant process, the efficiency is shout 1 ()%, or almost 50 time.s more efficient.

CONCLUSIONS

We have attempted to give the reader a brief summary of what we currentl y know about the solar and interplanetary causes of magnetic storms. '1'here are still quite a few voids in our knowledge and thus limitations in our ability to predict such events based on solar observations alone. We believe that within the near future there should be major advancements in our understanding of storms and the eventual ability to predict them in a quantitative fashion.

A *cknowledgments.* Portions of this research was done at the Jet Propulsion Laboratory under contract with National Aeronautics and Space Administration. We also wish to thank the National oceanic and Atmospheric Administration, Boulder, Colorado for their kind support in hosting one of us (B. 'l'. 'l'.) for a visit during the summer of 1993.

REFERENCES

Akasofu, S.-I., Energy coupling between the solar wind and the magnetosphere, Space Sci. Rev., 28, 121, 1981.

Axford, W. 1. and C. (). Hines, A unifying theory of high-latitude geophysical phenomena and geomagnetic S1OI"IIIS, Can. J. Phys., 39, 1433, 1961.

Burlaga, L. F., Magnetic Clouds, in Phys. of the Inner Heliosphere II, ed. R. Schwenn and E. Marsch, 1, Springer-Verlag Berlin, 1991.

Burlaga, L. P., K. W. Behannon and L. W. Klein, Compound streams, magnetic clouds, and major geomagnetic stem, J. Geophys. Res., 92, S725, 1987.

Choe, G. S., N. LaBelle-Hamer, B. 'l'. Tsurutani and 1,. C. 1 ee, Identification of a driver gas boundary layer, EOS, 73, 485, 1992.

Crooker, N. U., E. W, Cliver and B. T. Tsurutani, The semiannual variation of great geomagnetic storms and the postshock l<llssc:ll-h4cl'llc]-[et] effect preceding coronal mass ejecta, Geophys. Res. Lett., 19, 429, 1992.

Gonzalez, W. D., B. T. Tsurutani, A. L. C. Gonzalez, E. J. Smith, F. Tang and S.-I. Akasofu, Solar wind-magnetosphere coupling during intense magnetic storms, J. Geophys. Res., 94, 8835, 1989.

Gonzalez, W. D. A. L. C. Gonzalez and B. T. Tsurutani, Comment, Geophys. Res. Lett., 20, 1659, 1993.

Gonzalez, W. D. and B. 'J'. Tsurutani, Criteria of interplanetary parameters causing intense magnetic storms (D_{ST} < -100 n T), Planet. Space Sci., 35, 1101, 1987.

Gonzalez, W. 1>. and B. T. Tsurutani, Terrestrial response to eruptive solar flares: geomagnetic storms, in Eruptive Solar Flares, cd. by Z. Svestka, B. V. Jackson, M. E. Machado, Springer Verlag, 277, 1992.

Gonzalez, W. D. and B. T. Tsurutani, Interplanetary-magnetosphere coupling from ISEE-3, Proc. Sol. Terr. Energy Prog. (STEP) Symp., Ed. D. Baker, M. Teague and V. Papitashvili, Pergammon Press, 1993.

Gosling, J. T., D. N. Baker, S. J. Bame, W. C. Feldman, R. D. Zwickl and E. J. Smith, Bidirectional solar wind electron heat flux events, J. Geophys. Res., 92, 8519, 1987.

Gosling, J. 'J'., D. J. McComas, J. L. Phillips and S. J. Bame, Geomagnetic activity associated with Earth passage of interplanetary shock disturbances and coronal mass ejections, J. Geophys. Res., 96, 7831, 1991.

1 larrison, R. A., Solar coronal mass ejections and flare.s, Astron. Astrophys. 162, 283, 1986.

Harrison, R. A., Coronal transients and their relation to solar flares, Adv. Space Res., 11, 25, 1991.

1 loeksema, J. 'J'. and 1'.11. Scherrer, The solar magnetic field - 1976 through 1985, World I Data Report UAG-94, J 986.

1 locksema, J. "1'. and X. Zhao, Prediction of magnetic orientation in drive.r gas associated - B_Z events, J. Geophys. Res., 97, 3151, 1992.

Holzer, R. E. and J. A. Slavin, Magnetic Flux transfer associated with expansions and contractions" of the dayside magnetosphere, J. Geophys. Res., $3,3831, 1978.

Hundhausen, A, J., Sims and locations of Coronal Mass Ejections: SMM observations from 1980 and 1984-1989, J. Geophys. Res., 98, 1317'7, 1993.

Illing, R. M. E. and A. J. Hundhausen, Disruption of a coronal streamer by an eruptive prominence and a coronal mass ejection, J. Geophys. Res., 91, 10951, 1986.

Klein, L. W. and L. F. Burlaga, Interplanetary magnetic clouds at 1 AU, J. Geophys. Res., 87, 613, 1982.

1 ow, B. C. and D. F. Smith, The free energies of partially open coronal magnetic fields, Ap. J., 410, 412, 1993.

Marubashi, K., Interplanetary magnetic clouds and solar filaments, Adv. Space Res., 6, 335, 1986.

Russell, C. '1". and R. L. McPherron, Semiannual variation of geomagnetic activity, J. Geophys. Res., 78, 92, 1973.

Sibeck, D. G., R. E. Lopez and E. C. Roelof, Solar wind control of the magnetopause shape, location" and motion, J. Geophys. Res,, 96, 5489, 1991.

Sonnerup, B. U. and C. J. Cahill, Jr., Magnetopause structure and attitude from Explorer 12 observations, J. Geophys. Res., 72, 171, 1967.

Spreiter , J. R., A. L. Summers, and A. Y. Alkesne, Hydromagnetic flow around the magnetosphere, Planet. Space Sci., M, 223, 1966.

Tsurutani, B. T., W. D. Gonzalez, F. Tang, S.-1. Akasofu, and E. J. Smith, Origin of interplanetary southward magnetic field responsible for major magnetic storms near solar maximum (1978-1 979), J. Geophys. Res., 93, 8519, 1988.

Tsurutani, B. T., W. D. Gonzalez, Ii. Tang and Y. "1'. 1 ee, Great magnetic storms, Geophys. Res. Lett., 19, 73, 1992.

Tang, F., B. T. Tsurutani, W. D. Gonzalez, S.-1. Akasofu and E. J. Smith, Solar source of interplanetary southward Bz events responsible for major magnetic storms (1 978-1979), J. Geophys. Res., 94, 3535, 1989.

Zhao, X. 1'., J. '1'. Hocksema, J. '1'. Gosling and J. L. Phillips, Statistics of IMF Bz events, to appear in J. Geophys. Res., 1993.

Zwan, B. J. and R. A, Wolf, Depletion of the solar wind plasma near a planetary boundary, J. Geophys. Res., 3.1$_s$1636, 1976.

Zwickl, R. D., J. R. Asbridge, S. J. Bame, W. C. Feldman, J. '1'. Gosling, and E. J. Smith, Plasma properties of driver gas following interplane tary shocks observed by ISEE i-3, Solar Wind I ive, NASA Conf. Publ., CP-2280, '711 , 1983.

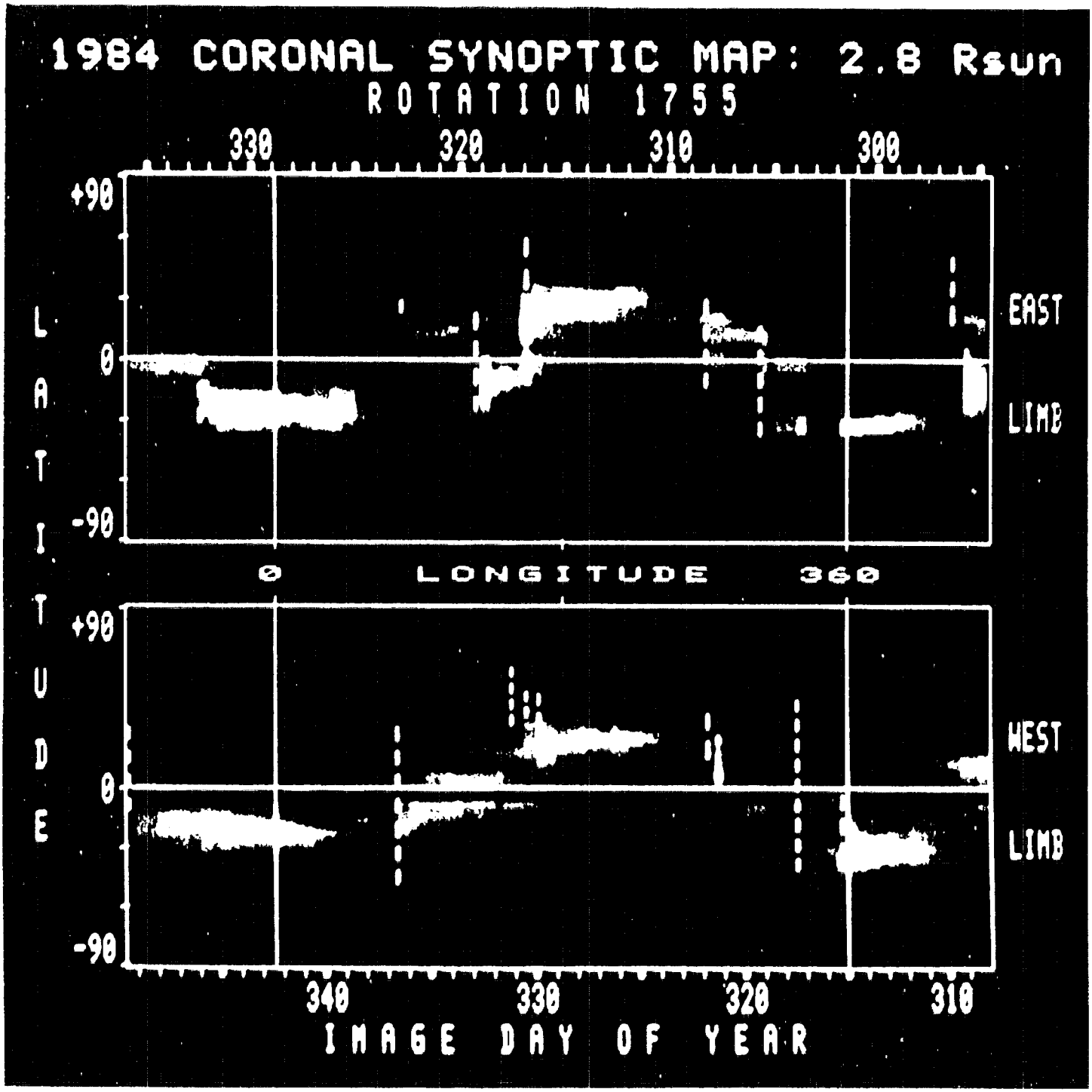
1984 CORONAL SYNOPTIC MAP: 2.8 Rsun
ROTATION 1755
330
320
310
300
+90
0
-90
LATITUDE
EAST
LIMB
0
LONGITUDE
360
+90
0
-90
LATITUDE
WEST
LIMB
340
330
320
310
IMAGE DAY OF YEAR

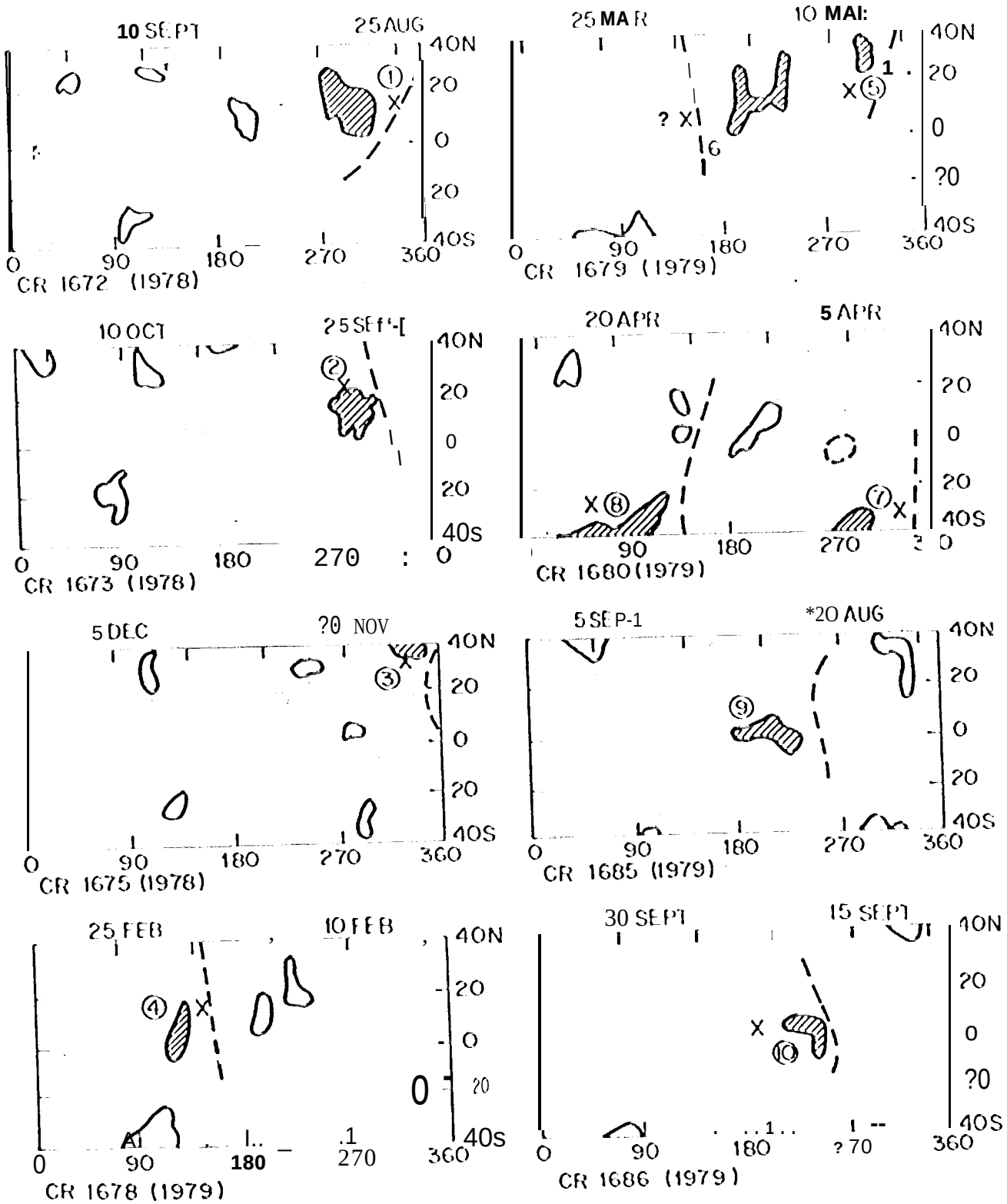

Solar Carrigton rotation maps with CI IARCS centers for the ten intense storm c.vents of the August 1978 -December 1979 interval. See text for details.

Fig 2

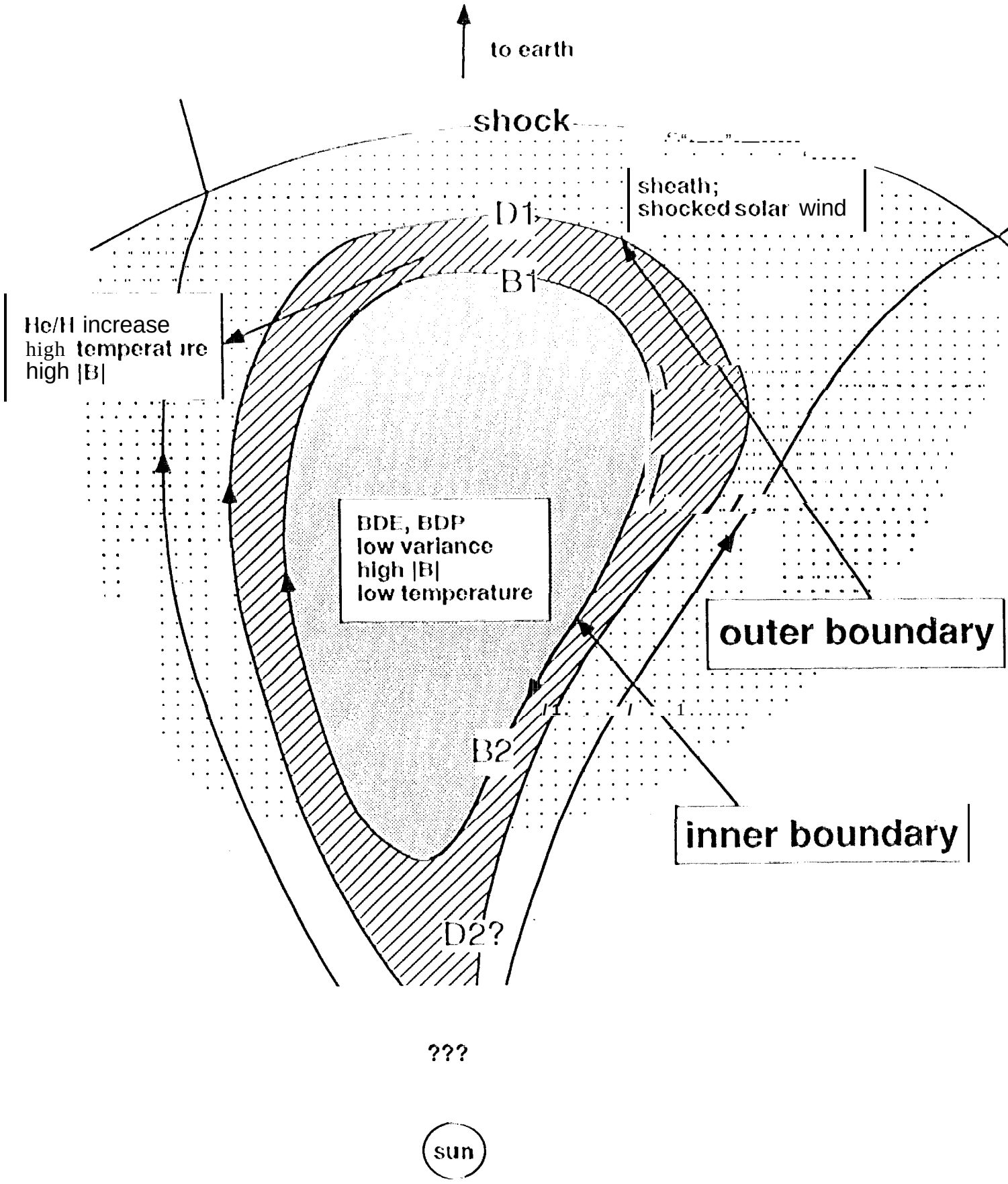
to earth
shock
sheath;
shocked solar wind
D1
B1
He/H increase
high temperature
high |B|
BDE, BDP
low variance
high |B|
low temperature
outer boundary
B2
inner boundary
D2?
???
sun

Fig 3

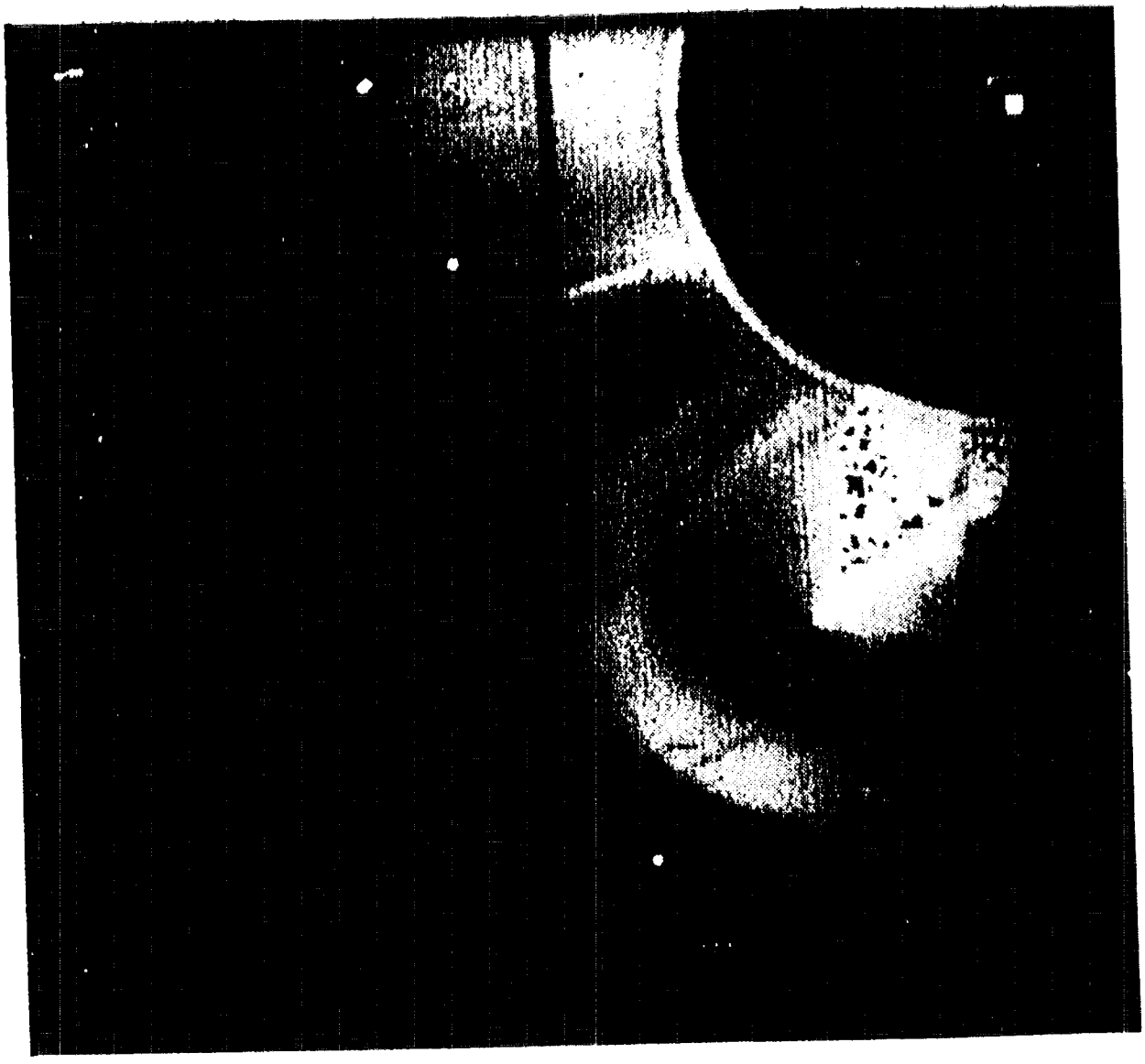

ILLING AND HU NDHAUSEN, 1986.

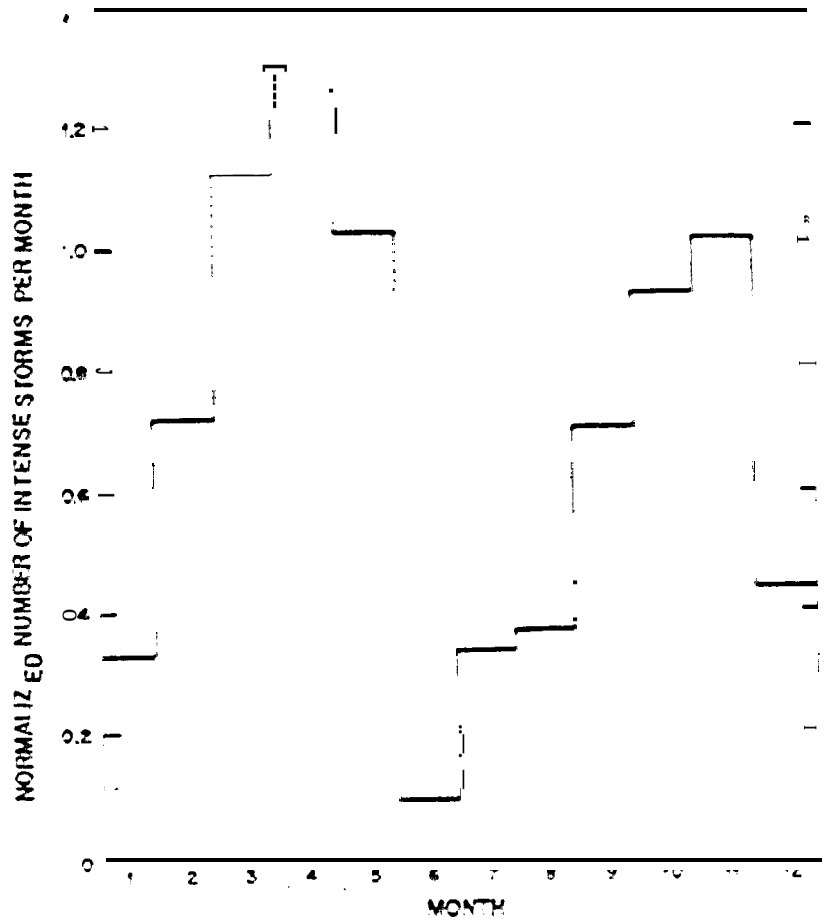

Seasonal distribution of intense storms ($Dst < -100$ nT) for the interval 1975–1986. The normalized number of these storms per month is given.

SHEATH FIELDS

a) Shocked southward fields
'1 surutani et. al., 1988

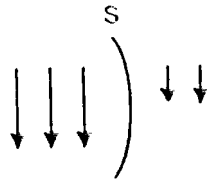

b) Shocked heliospheric current sheets
'1 surutani et. d., 1984

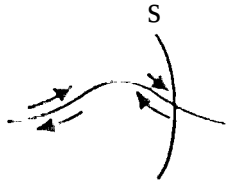

c) '1 urbulence, waves or discontinuities

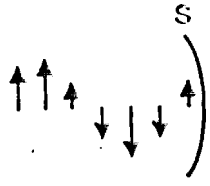

d) Draped magnetic fields
Zwan and Wolf, 19-/G

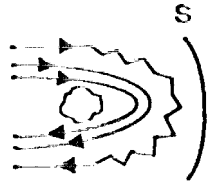

c) McComas et. al., 1989

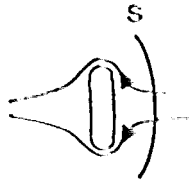

f) Russell and McPherron, 1973;
Crooker et. al., 1992

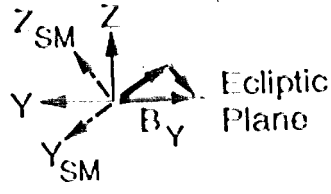

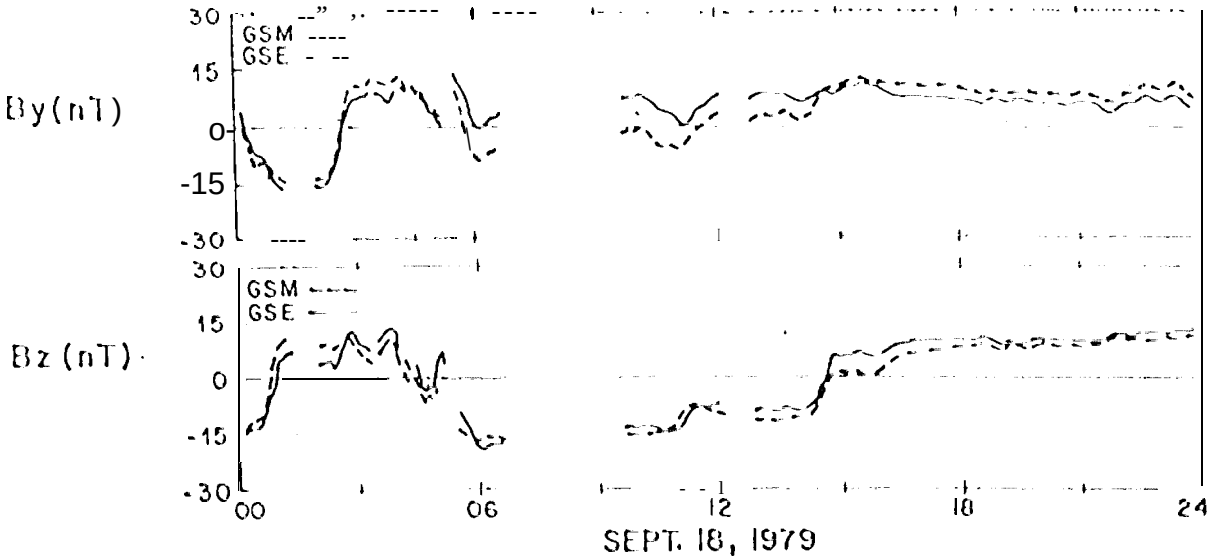
By(nT)
Bz (nT)
GSM
GSE
30
15
0
-15
-30
00
06
12
18
24
SEPT. 18, 1979

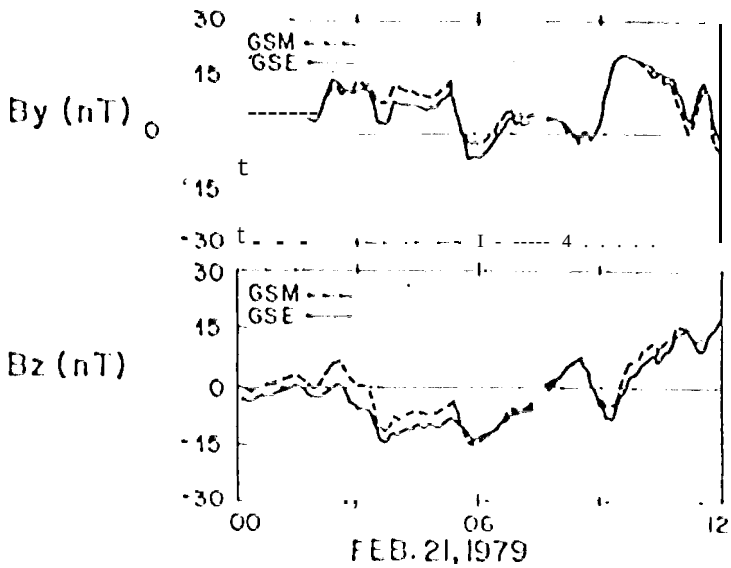
By (nT)
Bz (nT)
GSM
GSE
30
15
0
-15
-30
00
06
12
FEB. 21, 1979

Fig 7

LOCATION OF SOLAR SOURCES FOR DRIVER GAS EVENTS CAUSING INTENSE ($D_{ST} \leq -100nT$ AND GREAT ($D_{ST} \leq -250nT$) STORMS*

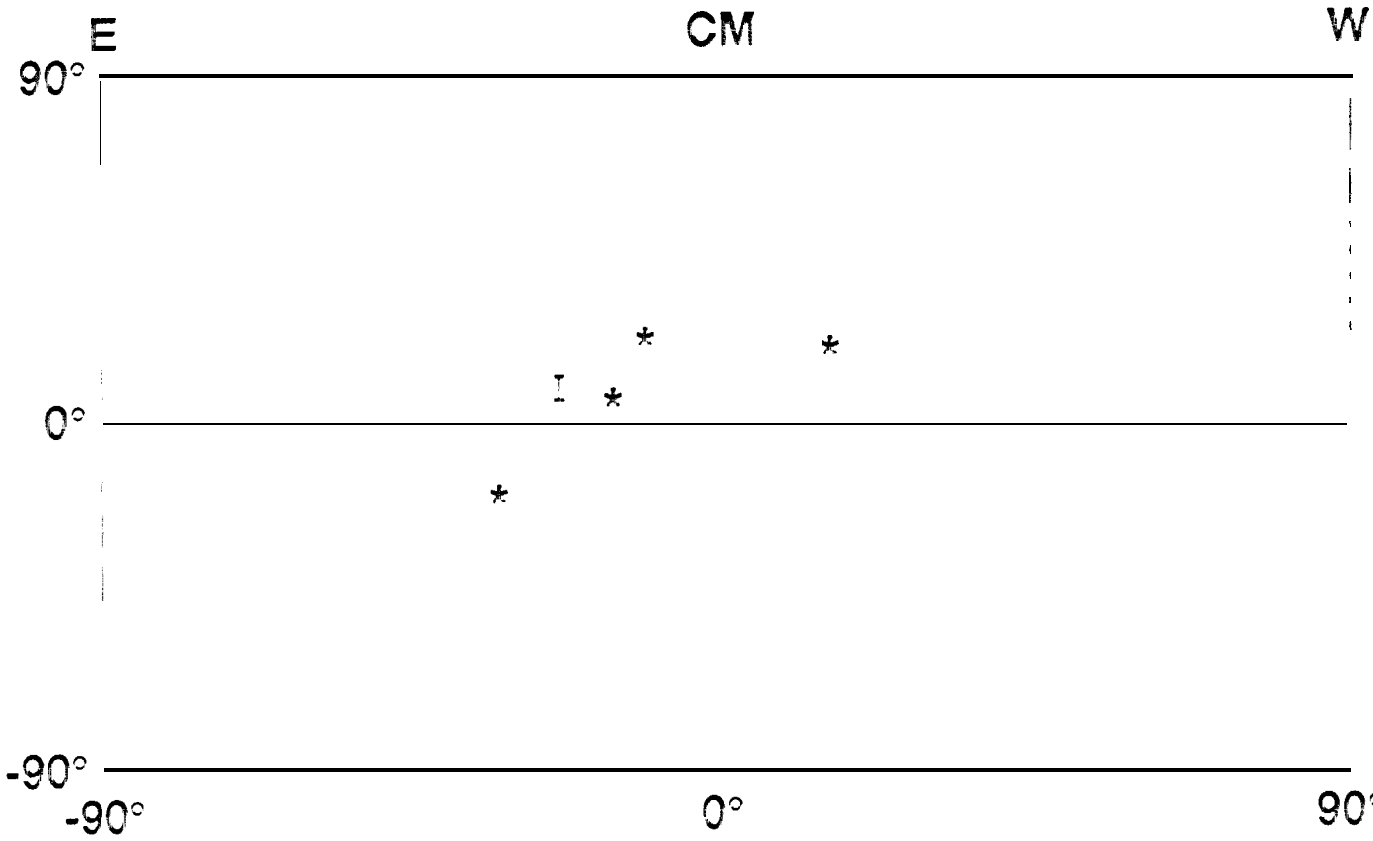

DATE	EVENT	LOCATION
AUG 27, 1978	8° N	15° E
SEPT 29, 1978	20° N	18° W
FEB 21, 1979	22° N	10° E
APRIL 4, 1979	19° S	31° E
DEC 19, 1980	6°-12° N	24° E

* LATITUDE OF EARTH SUBTRACTED OUT

CONCENTRIC HELICAL MAGNETIC FIELDS AT CMEs

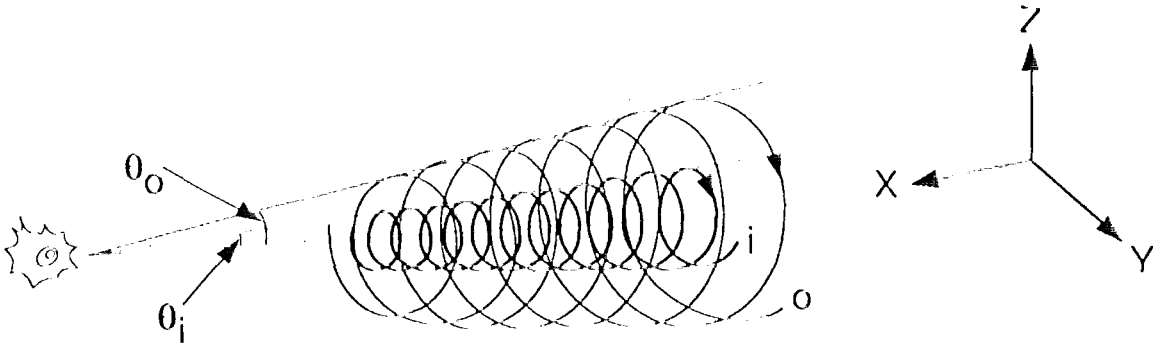

$B_i > B_o$

$\theta_i < \theta_o$

i = INNER LOOP
o = OUTER LOOP

Fig 9

ONLY FRACTIONS OF $\theta = \theta_0$ CONTAIN SUBSTANTIAL B_Z

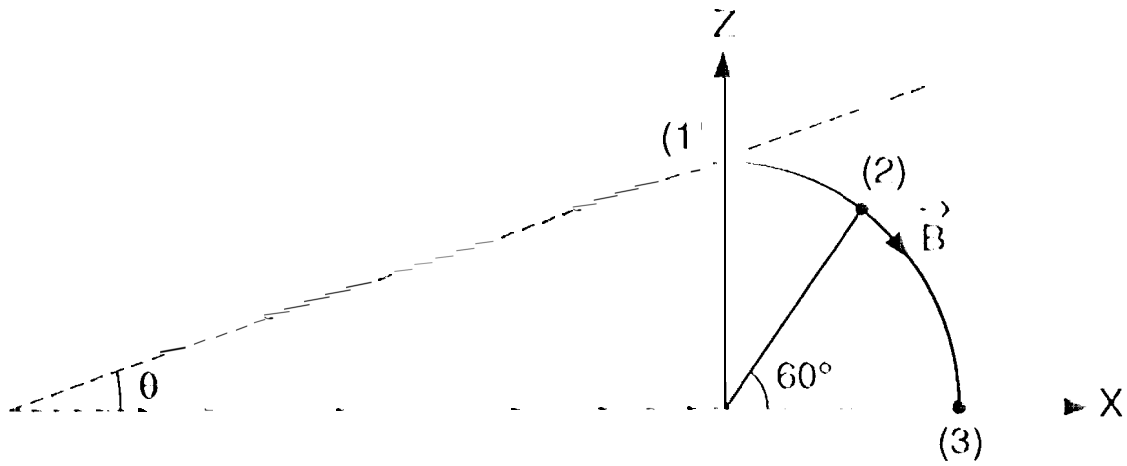

AT (1) $B_X = B$, $B_Z = 0$

(2) $B_X = 0.3|B|$, $B_Z = 0.7\,B$

(3) $B_X = 0$, $B_Z = |B|$

INTENSE STORMS (-220 nT < peak Dst < -100 nT)

EVENT	Bz GSE (nT)	Bz GSM (nT)	Increment (%)
Aug. 28, 1978	-22.0	-24.5	11.4
Sep. 29	-26.0	-22.1	-15.0
Nov. 25	-16.2	-17.0	4.9
Feb. 21, 1979	-14.1	-15.7	11.3
Mar. 10	-12.4	-1s.0	21.0
Mar. 29	-9.7	-10.9	12.4
Apr. 4	gap		
Apt, 25	gap		
Aug. 29	-13.8	-1?.1	-12.3
Sep. 18	-19.3	-17.4	-9.8

GREAT STORMS (pink Dst <-250 nT)

EVENT	Bz GSE (nT)	Bz GSM (nT)	Increment (%)
Dec. 19, 1980	-14.1	-15.0	6.4
Apr. 13, 1981	-30,7	-23.2	-24.4
Jul. 13, 1982	-35,4	-34.5	-?..5
Sep. 6,1982	-2.().8	-20.3	-2.4
Feb. 7, 1986	uncertain		

Table 1

SUMMARY OF PARAMETERS RELATED TO THE 11 POSITIVE B_Z EVENTS. SEE TEXT FOR DETAILS

	Date (U.T.)	Peak B_N (nT)	Duration (h)	Peak |B| (nT)	Shock-Relationship: Mach number	Lag (h)	AE (nT)	D_{ST} (nT)	V (km s^{-1})	ρ_p (cm^{-3})	ρ_{He} (cm^{-3})	B_y (nT)
1.	18 December 1978 (0100)	15	3	26	---	NCDE	0	0	450	10.0	0.8	-12,+14
2.	21 February 1979 (1200)	20	4	22	2.2	9	75	R	560	12.0	0.4	+22
3.	3 April (1230)	12	3	14	1.0	37	75	R	440	8.0	0.4	-4
4.	5 April (0300, 1800)	20	4	33	2.9	0	200	R	605	11.0	1.0	-10,+20
5.	5 April (1230)	30	4	40	2.9	9	300	0	695	15.0	1.1	-8,+18
6.	30-31 May (2130)	15	3	23	2.2	3.5		0±	750	20.0	1.0	+8
7.	20 August (0830)	18	6	30	1.7	0	150	0±	670	13.0	0.4	25, +5
8.	18-19 September (2400)	12	3	15	---	NCDE	35	R(Q)	365	12.0	0.8	+6.5
9.	6 October (1800)	18	3	20	2.1	6.5	110	R	370	45.0	2.0	+10,-10
10.	7 October (0800)	16	4	20	2.1	19	350(v)	R	425	12.0	0.2	+4
11.	11 November (1800)	20	6	23	2.5	12.5	100	0±	450	12.0	0.8	+12,-10

Table 1.

SUMMARY OF PARAMETERS RELATED TO THE 11 POSITIVE B_Z EVENTS

	$(\rho_H + \rho_{He}) V_{SW}^2$	B_{mp} (nT)	R_{SO} R_E (6380 km) nose	flank	Area (cm^2)	$1/2MN V_{SW}^3$ (erg cm^{-2} s^{-1})	E_T erg s^{-1}
1.	4.5×10^{-8}	8.2×10^{-4}	9.0	9.9	1.3×10^{20}	1.0	1.3×10^{20}
2.	7.1×10^{-8}	1.0×10^{-3}	8.4	9.2	1.1×10^{20}	2.0	2.2×10^{20}
3.	3.1×10^{-8}	6.8×10^{-4}	9.6	10.6	1.4×10^{20}	0.7	1.0×10^{20}
4.	9.2×10^{-8}	1.2×10^{-3}	7.9	8.7	7.0×10^{19}	2.8	2.0×10^{20}
5.	1.6×10^{-7}	1.5×10^{-3}	7.3	8.0	8.2×10^{19}	5.4	4.4×10^{20}
6.	2.3×10^{-7}	1.8×10^{-3}	6.9	7.6	7.4×10^{19}	8.5	6.3×10^{20}
7.	1.1×10^{-7}	1.3×10^{-3}	7.7	8.5	9.2×10^{19}	3.7	1.3×10^{20}
8.	3.4×10^{-8}	7.1×10^{-4}	9.5	10.5	1.4×10^{20}	0.6	8.4×10^{19}
9.	1.2×10^{-7}	1.3×10^{-3}	7.7	8.5	9.2×10^{19}	2.2	2.0×10^{20}
10.	3.9×10^{-8}	7.6×10^{-4}	9.2	10.1	1.3×10^{20}	0.8	1.0×10^{20}
11.	5.1×10^{-8}	8.7×10^{-4}	8.8	9.7	1.2×10^{20}	1.2	1.4×10^{20}

Continued. SUMMARY OF PARAMETERS RELATED TO THE 11 IMF B_N EVENTS.

	Emag erg s^{-1}	η efficiency
1.	---	...
2.	2.2×10^{17}	1.0×10^{-3}
3.	2.2×10^{17}	2.2×10^{-3}
4.	6.0×10^{17}	3.0×10^{-3}
5.	9.0×10^{17}	2.0×10^{-3}
6.	---	...
7.	$4.5X\ 10^{17}$	3.4×10^{-3}
8.	1.1×10^{17}	1.3×10^{-3}
9.	3.3×10^{17}	1.7×10^{-3}
10.	1.1×10^{18}	1.1×10^{-2}
11.	3.0×10^{17}	2.1×10^{-3}

Table 3